

Method of separated form factors for polydisperse vesicles

Jeremy Pencer, Susan Krueger, Carl P. Adams and John Katsaras

Copyright © International Union of Crystallography

Author(s) of this paper may load this reprint on their own web site provided that this cover page is retained. Republication of this article or its storage in electronic databases or the like is not permitted without prior permission in writing from the IUCr.

Method of separated form factors for polydisperse vesicles

Jeremy Pencer,^{a,b*} Susan Krueger,^c Carl P. Adams^b and John Katsaras^{a,d}

Received 15 November 2005

Accepted 14 February 2006

^aNational Research Council, Canadian Neutron Beam Centre, Chalk River Laboratories, Building 459, Station 18, Chalk River, ON, K0J 1J0, Canada, ^bDepartment of Physics, St Francis Xavier University, Antigonish, NS, B2G 2W5, Canada, ^cNIST Center for Neutron Research, National Institute of Standards and Technology, 100 Bureau Drive, Stop 8562, Bldg 235/Room E151, Gaithersburg, MD 20899-8562, USA, and ^dDepartment of Physics, Guelph Waterloo Physics Institute and Biophysics Interdepartmental Group, University of Guelph, Guelph, ON, N1G 2W1, Canada. Correspondence e-mail: jeremy.pencer@nrc.gc.ca

Use of the Schulz or Gamma distribution in the description of particle sizes facilitates calculation of analytic polydisperse form factors using Laplace transforms, $\mathcal{L}[f(u)]$. Here, the Laplace transform approach is combined with the separated form factor (SFF) approximation [Kiselev *et al.* (2002). *Appl. Phys. A*, **74**, S1654–S1656] to obtain expressions for form factors, $P(q)$, for polydisperse spherical vesicles with various forms of membrane scattering length density (SLD) profile. The SFF approximation is tested against exact form factors that have been numerically integrated over the size distribution, and is shown to represent the vesicle form factor accurately for typical vesicle sizes and membrane thicknesses. Finally, various model SLD profiles are used with the SFF approximation to fit experimental small-angle neutron scattering (SANS) curves from extruded unilamellar vesicles.

© 2006 International Union of Crystallography
Printed in Great Britain – all rights reserved

1. Introduction

In biological systems, membranes play an essential role as selectively permeable barriers and as platforms for locating delivery and exchange systems (Alberts *et al.*, 1989). Since they are more easily characterized than their more complex biological counterparts, yet share many of the same properties, unilamellar vesicles (ULVs) are frequently used as model membrane systems. ULVs also have an important role as capsules for drug delivery (Gregoriadis, 1995), and have been utilized as reaction compartments for the controlled synthesis of nanometre-sized crystals (Korgel & Monbouquette, 2000). ULVs, shown schematically in Fig. 1, are essentially hollow shells, suspended in and containing aqueous media. The ULV shell (also shown schematically in Fig. 1) is composed of a lipid bilayer membrane, which has a hydrophilic surface (composed of lipid headgroups) and hydrophobic interior (composed of hydrophobic lipid tails).

Over the years, there have been a wide variety of studies to characterize membrane structure, hydrophobic thickness and interfacial hydration (*e.g.* Worcester & Franks, 1976; Hristova & White, 1998; Marsh, 2002). Typically, these studies have been motivated by the potential importance of membrane thickness in modulating protein insertion (Ridder *et al.*, 2002), activity (Ben-Shooshan *et al.*, 2002) and membrane lateral organization (Killian, 1998; Dumas *et al.*, 1999). Small-angle scattering (*e.g.* Wilkins *et al.*, 1971; Pencer & Hallett, 2000; Schmiedel *et al.*, 2001; Kiselev, Zbytovská *et al.*, 2004; Kiselev,

Zemlyanaya & Aswal, 2004; Kučerka *et al.*, 2004; Zbytovská *et al.*, 2005; Nieh *et al.*, 2005; Pencer, Nieh *et al.*, 2005) and diffraction studies (*e.g.* Worcester & Franks, 1976; King *et al.*, 1985; Jacobs & White, 1989; Katsaras *et al.*, 1992; Raghunathan & Katsaras, 1995; Marsan *et al.*, 1998; Darkes & Bradshaw, 2000) have proven to be particularly effective in providing information about the lipid bilayer hydrophobic thickness, degree of hydration, and influence on these parameters by additives such as steroids and hydrophobic solutes.

While the application of small-angle scattering to the study of membrane structure in vesicles or liposomes is certainly not new (*see e.g.* Wilkins *et al.*, 1971), structural studies on ULVs continue to garner interest. Recently, several different

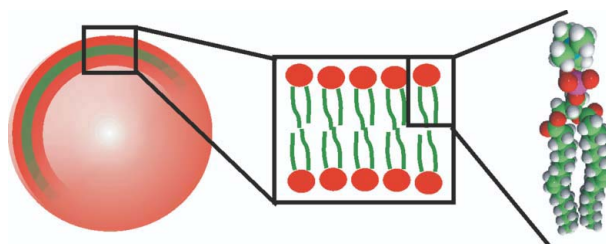


Figure 1
Schematic representation of a unilamellar vesicle (ULV) (left), lipid bilayer (middle) and typical phospholipid (right). In the left and center figures, the hydrophilic lipid heads are shown in red and hydrophobic tails are shown in green. In the space-filling model of a lipid on the right, C and N atoms are shown in green, O atoms in red, H atoms in white and P in magenta.

approaches have been applied to extract detailed membrane structural parameters from ULV SANS and small-angle X-ray scattering (SAXS) data (Schmiedel *et al.*, 2001; Riske *et al.*, 2001; Pabst *et al.*, 2003; Kiselev, Zemlyanaya & Aswal, 2004; Brzustowicz & Brunger, 2005). The SLD profiles of ULV membranes, in particular, have been successfully modeled using a ‘top-hat’ function or uniform shell (*e.g.* Pencer & Hallett, 2000), a series of uniform shells or sum of ‘top-hat’ functions (*e.g.* Riske *et al.*, 2001; Schmiedel *et al.*, 2001; Pencer, Mills *et al.*, 2005), a combination of layers of uniform and linearly varying SLD (*e.g.* Kučerka *et al.*, 2004) or sum of Gaussians (*e.g.* Pabst *et al.*, 2003; Brzustowicz & Brunger, 2005).

In extracting membrane structural parameters from SANS data, complications arise due to the polydispersity inherent in ULV preparations. Typically, polydispersity is taken into account in fits to SANS and SAXS data by numerical integration of the monodisperse form factor over the size distribution (*e.g.* Pencer & Hallett, 2000). The use of analytic polydisperse form factors (as in *e.g.* Wagner, 2004), on the other hand, provides a rapid way to fit experimental data *via* non-linear least-squares fitting.

Recently, the method of separated form factors (SFF) was introduced, which facilitates the incorporation of any arbitrary analytic or numerical SLD profile into the ULV scattering function (Kiselev *et al.*, 2002; Kiselev, Zbytovská *et al.*, 2004; Kiselev, Zemlyanaya & Aswal, 2004). Here, we take the previously derived monodisperse SFF (Kiselev *et al.*, 2002) and from it derive an analytic expression for the SFF for polydisperse ULVs whose sizes are distributed *via* the Schulz or Gamma distribution. Expressions for vesicle form factors are then derived using several proposed membrane SLD profiles. We test the accuracy of the polydisperse SFF approximation against the exact form factor using the polydisperse uniform-shell model (Bartlett & Ottewill, 1992). The SFF is also tested against exact monodisperse form factors that have been numerically integrated over the size distribution. Finally, experimental SANS data from ULV samples of differing chemical or isotopic composition are fitted, in order to compare the various SLD models.

2. Theory

The intensity of neutrons scattered from a polydisperse ensemble of interacting particles is given by (Kotlarchyk & Chen, 1983)

$$I(q) = n_p \langle P(q) \rangle S'(q), \quad (1)$$

where n_p is the particle number density, $\langle P(q) \rangle$ denotes the size distribution average of the monodisperse particle form factor, $P(q) = |F(q)|^2$, $F(q)$ is the scattering amplitude, and $S'(q)$ is the polydisperse structure factor. $S'(q)$ is given by

$$S'(q) = 1 + \beta(q)[S(q) - 1], \quad (2)$$

where

$$\beta(q) = \langle |F(q)|^2 \rangle / \langle |F(q)|^2 \rangle, \quad (3)$$

$S(q)$ is the monodisperse structure factor, and the scattering vector value, q , is defined by $q = 4\pi \sin(\theta/2)/\lambda$, where θ is the scattering angle and λ is the wavelength of the incident beam.

2.1. The monodisperse form factor

By symmetry considerations, the Fourier transform of the SLD for spherical shells, or vesicles, can be written as a radial integral. The monodisperse form factor, $P(q) = [F(q)]^2$, is then calculated as

$$P(q) = [F(q)]^2 = (4\pi)^2 \left\{ \int_0^\infty [\rho(r) - \rho_m] r^2 \frac{\sin(qr)}{qr} dr \right\}^2, \quad (4)$$

where $\rho(r)$ is the SLD as a function of the radial distance from the center of the vesicle, and ρ_m is the SLD of the medium. Note that F and P are functions of the vesicle radius, R , membrane thickness, t , and SLD, ρ , as well as q .

2.2. The method of separated form factors (SFF)

Recently, an approximation to the vesicle form factor, $P(q)$, the SFF approximation, had been introduced which takes advantage of the small magnitude of the membrane thickness compared with the vesicle radius, a characteristic feature of phospholipid vesicles (Kiselev *et al.*, 2002).

In the derivation of the SFF approximation, the integral form of the monodisperse vesicle scattering amplitude, $F(q, R)$, is rewritten in terms of the vesicle radius, R , to give (Kiselev *et al.*, 2002)

$$F(q, R) = 4\pi \int_{-t/2}^{t/2} [\rho(x) - \rho_m] \frac{\sin[(R+x)q]}{(R+x)q} (R+x)^2 dx, \quad (5)$$

where $x = 0$ corresponds to the bilayer midplane, the membrane SLD $\rho(x) \neq \rho_s$ for $-t/2 < x < t/2$, where ρ_m is the SLD of the medium, and R corresponds to the vesicle radius, or distance from the vesicle center to the bilayer midplane. When the membrane thickness, t , is much less than R , we have that $R \gg t/2$ and $R+x \simeq R$. For symmetric bilayers, the scattering amplitude can then be approximated by (Kiselev *et al.*, 2002)

$$F(q, R) \simeq F_{\text{SFF}}(q, R) = 4\pi R^2 \frac{\sin(qR)}{qR} \int_{-t/2}^{t/2} [\rho(x) - \rho_m] \cos(qx) dx. \quad (6)$$

The error, or difference between the approximate and exact scattering functions, introduced by the SFF approximation to the exact form factor is not discussed here, as it has been dealt with, in detail, by Kiselev *et al.* (2002). Comparison of F_{SFF} with the form factors for planar membranes (*e.g.* Pencer & Hallett, 2000) and infinitely thin shells (*e.g.* Pencer & Hallett, 2003) shows that F_{SFF} can be written as (Kiselev *et al.*, 2002)

$$F_{\text{SFF}}(q, R) = F_{\text{TS}}(q, R) F_{\text{M}}(q), \quad (7)$$

where the thin-shell scattering amplitude, F_{TS} is given by

$$F_{\text{TS}}(q, R) = 4\pi R^2 \frac{\sin(qR)}{qR}, \quad (8)$$

and the scattering amplitude from the membrane, F_{M} , is given by

$$F_{\text{M}}(q) = \int_{-t/2}^{t/2} [\rho(x) - \rho_{\text{m}}] \cos(qx) dx. \quad (9)$$

Note that the membrane form factor for randomly oriented flat sheets, which can be used to approximate the scattering from large vesicles with high polydispersity, given by *e.g.* Pencer & Hallett (2000), is similar to the expression given in equation (9), except that it also includes a Lorentz correction, $1/q$, resulting in

$$F_{\text{KP}}(q) = \frac{1}{q} \int_{-t/2}^{t/2} [\rho(x) - \rho_{\text{m}}] \cos(qx) dx. \quad (10)$$

This expression is often referred to as the Kratky–Porod approximation (*e.g.* Pencer & Hallett, 2000, and references therein).

2.3. The Laplace method

The Schulz distribution has been used successfully to describe the size distribution of a variety of colloidal aggregates (Aragón & Pecora, 1976; Hayter, 1983; Kotlarchyk & Chen, 1983; Bartlett & Ottewill, 1992; Wagner, 2004). As demonstrated by electron microscopy (Hallett, Nickel *et al.*, 1991), light scattering (Hallett, Watton & Krygsmann, 1991) and SANS (Pencer, Mills *et al.*, 2005), the size distribution of extruded phospholipid vesicles is well described by a Schulz distribution. Despite the successful use of the Schulz and other similar continuous functions to describe vesicle size distributions, some caution should be exercised to avoid the use of non-physical parameters (*e.g.* excessively large polydispersity) which lead to distributions where vesicles can have radii smaller than their thickness, *i.e.* $R < t$.

For polydisperse particles whose sizes follow a Schulz distribution, it has been recognized elsewhere that the polydisperse form factor can be expressed in terms of a Laplace transform of the monodisperse form factor (Aragón & Pecora, 1976; Hayter, 1983; Kotlarchyk & Chen, 1983; Bartlett & Ottewill, 1992; Wagner, 2004). Below, we show the application of the Laplace transform method to the SFF approximation for Schulz-distributed vesicles.

The polydisperse form factor is determined by integrating the monodisperse form factor, $P(q)$, over the Schulz distribution, resulting in

$$P_z(q) = \int_0^\infty [F(q, R)]^2 G(R) dR, \quad (11)$$

and polydisperse scattering amplitude

$$F_z(q) = \int_0^\infty F(q, R) G(R) dR, \quad (12)$$

where the Schulz distribution, $G(R)$, is given by

$$G(R) = \left(\frac{z+1}{R_a}\right)^{z+1} \frac{R^z}{\Gamma(z+1)} \exp\left[-\frac{R(z+1)}{R_a}\right], \quad (13)$$

the mean radius is R_a , the variance is $\sigma^2 = R_a^2/(z+1)$ and the polydispersity (or relative variance) is $1/(z+1)$.

A potential problem in the use of the SFF approximation with a polydisperse population of vesicles relates to the possible breakdown of the validity of the SFF, since, even though $t < R_a$, R could span a range of values where $t \geq R$. Thus, in order for the SFF to remain valid, we have the additional requirement that $t < R_a - 2\sigma$. Values of R less than $R_a - 2\sigma$ are not important, since the value of $G(R)$ in this range is negligible (see *e.g.* Aragón & Pecora, 1976).

Letting $u = R$ and $s = (z+1)/R_a$, we find

$$\begin{aligned} P_z(q) &= g_1 \int_0^\infty u^{sR_a-1} [F(q, u)]^2 \exp(-su) du \\ &= g_1 \mathcal{L}\{u^{sR_a-1} [F(q, u)]^2\}, \end{aligned} \quad (14)$$

where \mathcal{L} is the Laplace transform operator and $g_1 = [(z+1)/R_a]^{z+1} [\Gamma(z+1)]^{-1}$. Similarly, the size distribution average of the scattered amplitude, $F(q)$, can be calculated:

$$F_z(q) = g_1 \mathcal{L}\{u^{sR_a-1} F(q, u)\}. \quad (15)$$

In principle, it is possible to use equations (14) and (15) to determine analytic forms for both $\langle P(q) \rangle$ and $\beta(q)$ for a variety of membrane SLD profiles in spherical vesicles. However, even for relatively simple profiles (such as the three-layer rectangular profile discussed below) the complexity of such expressions precludes their utility. The SFF approximation greatly simplifies matters, since, in the SFF expression, the membrane SLD no longer depends on the vesicle radius. Since F_{M} is independent of R , substitution of equation (7) into equation (14) results in

$$P_z(q) = g_1 [F_{\text{M}}(q)]^2 \mathcal{L}\{u^{sR_a-1} [F_{\text{TS}}(q, u)]^2\}. \quad (16)$$

Similarly, substitution of equation (7) into equation (15) gives

$$F_z(q) = g_1 F_{\text{M}}(q) \mathcal{L}\{u^{sR_a-1} F_{\text{TS}}(q, u)\}. \quad (17)$$

Evaluation of the Laplace transform in equation (16) results in

$$\begin{aligned} P_z(q) &= \langle P(q) \rangle \\ &= \frac{8\pi^2(z+2)(z+3)}{s^2 q^2} [F_{\text{M}}(q)]^2 \\ &\quad \times \left\{ 1 - \frac{(1+4q^2/s^2)^{-(z+1)/2} s^2 \cos[(3+z) \arctan(2q/s)]}{4q^2 + s^2} \right\}. \end{aligned} \quad (18)$$

The evaluation of F_z follows similarly to give

$$F_z(q) = \frac{4\pi(z+1)(z+2)(z+3)}{q} F_M(q) \times \frac{(1+q^2/s^2)^{-z/2} s \sin[(4+z) \arctan(q/s)]}{(q^2+s^2)^2}. \quad (19)$$

In the following section, we derive expressions for F_M for a number of commonly used model membrane SLD profiles.

2.4. Membrane form factors

Models for or approximations to membrane SLD profiles, typically consist of one or several ‘rectangular’ or ‘top-hat’ functions (*e.g.* King *et al.*, 1985; Pencer & Hallett, 2000; Schmiedel *et al.*, 2001; Riske *et al.*, 2001), or one or several Gaussians (Wiener & White, 1992; Nagle & Tristram-Nagle, 2000; Pabst *et al.*, 2003; Brzustowicz & Brunger, 2005). Below, we first derive expressions for the scattering amplitudes for profiles based on the ‘top-hat’ representation as well as some recent extensions to this model, followed by those for the sum of Gaussians representation. These model SLD profiles are shown schematically in Fig. 2 for conditions corresponding to neutron scattering contrast of hydrogenous lipid in pure D₂O.

It should be noted that the SLD profiles appropriate for SAXS are quite different from those shown for lipid in D₂O. In general, there exists the opportunity to accentuate or reduce the scattering contribution from the various lipid components by the appropriate choice of probe (either X-ray or neutron) or, in the case of neutron scattering, the isotopic composition of either the lipid or medium. For example, the high electron density of the phosphate portions of the lipid headgroups

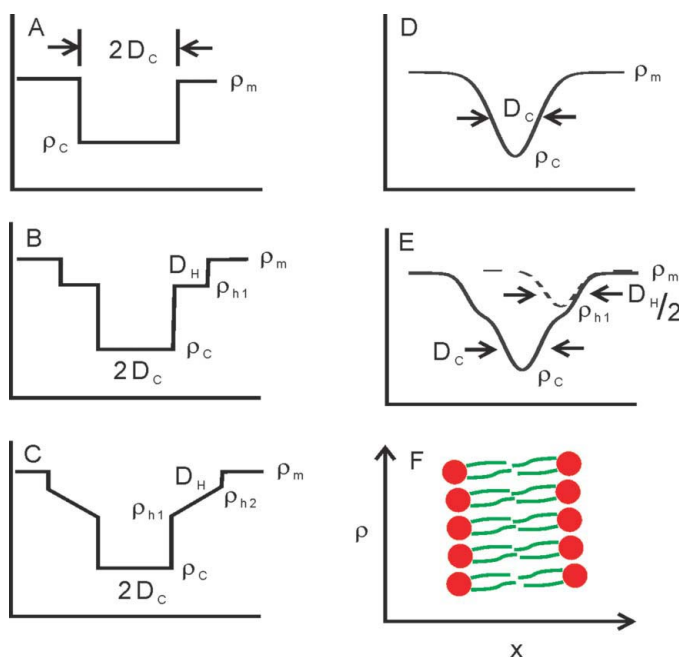


Figure 2 Schematic representation of various model SLD profiles for the lipid bilayer membrane. (A) A membrane with uniform SLD. (B) Three shells with uniform SLD. (C) Three shells with linearly varying SLD. (D) A single Gaussian SLD profile. (E) A profile equal to a sum of three Gaussians. (F) Schematic representation of a lipid bilayer, showing the orientation and position of lipids relative to the SLD plots.

Table 1

Molecular volumes, V , X-ray and neutron scattering lengths, b , and scattering length densities, ρ , for DPPC at 323 K.

The X-ray SLD of H₂O (and D₂O) is 0.95 fm \AA^{-3} and neutron SLDs are -0.056 and 0.64 fm \AA^{-3} for H₂O and D₂O, respectively.

	DPPC	Headgroup	Acyl chains	Deuterated chains
Chemical formula	C ₄₀ H ₈₀ NO ₈ P	C ₁₀ H ₁₈ NO ₈ P	C ₃₀ H ₆₂	C ₃₀ D ₆₂
V (\AA^3)	1232	319	913	913
B (fm, X-ray)	1146	465.7	682.9	682.9
B (fm, neutron)	27.6	60.1	-32.4	613
ρ (fm \AA^{-3} , X-ray)	0.93	1.46	0.748	0.748
ρ (fm \AA^{-3} , neutron)	0.023	0.188	-0.036	0.671

make these the primary contributor to the X-ray scattering signal from the lipid, as opposed to the negative SLD of the acyl chains which gives the largest contribution to the neutron scattering signal from lipid in D₂O in Fig. 2. In Table 1, neutron and X-ray scattering lengths and densities are shown for DPPC (1,2-dipalmitoyl-sn-glycero-3-phosphocholine). Scattering lengths are determined from the atomic scattering lengths (Sears, 1992), and corresponding scattering length densities are calculated from the scattering lengths and known molecular or component volumes (Nagle & Tristram-Nagle, 2000; Pencer, Mills *et al.*, 2005). As can be seen from the SLD values summarized in Table 1, SANS measurements of hydrogenous lipid in D₂O are most sensitive to the contribution of the acyl-chain region, while SANS or SAXS measurements of hydrogenous lipid in H₂O will be more sensitive to the scattering contribution from the headgroup regions, and therefore also be sensitive to the spacing between them.

The ‘top-hat’ is the simplest of the models (Fig. 2A) for vesicle membranes, which assumes a uniform SLD, *i.e.* $\rho(x) = \rho_c$ when $-D_C < x < D_C$, and $\rho(x) = \rho_m$ when $x < -D_C$ or $D_C < x$, where $2D_C$ is the membrane hydrophobic thickness, ρ_c is the SLD of the membrane hydrophobic region and ρ_m is the SLD of the medium or solvent. The membrane scattering amplitude, F_M , for this profile is

$$F_M(q) = \frac{2(\rho_c - \rho_m)}{q} \sin(qD_C). \quad (20)$$

As has been observed in a number of studies (*e.g.* Kučerka *et al.*, 2004; Kiselev, Zemlyanaya & Aswal, 2004), the uniform-shell model, while adequately describing scattering from vesicles when $2qD_C < 1$, fails to reproduce the observed scattering behavior at higher q , due to the inhomogeneous SLD normal to the membrane surface. One way to account for such inhomogeneities is to represent the SLD profile by a multishell model (Fig. 2B), where scattering from the lipid acyl-chain and headgroup regions are treated separately (see Fig. 1). The membrane SLD, $\rho(x)$ is then defined as

$$\rho(x) = \begin{cases} \rho_h & \text{when } -D_C - D_H < x < -D_C, \\ \rho_c & \text{when } -D_C < x < D_C, \\ \rho_h & \text{when } D_C < x < D_C + D_H, \\ \rho_m & \text{when } |x| > D_H + D_C. \end{cases}$$

In this case, the scattering amplitude is given by

$$F_M(q) = 2(\rho_c - \rho_h) \frac{\sin(qD_C)}{q} + 2(\rho_h - \rho_m) \frac{\sin[q(D_H + D_C)]}{q}, \quad (21)$$

where ρ_h , ρ_c and ρ_m are the SLD of the headgroups, hydrocarbon tails, and medium, respectively, D_H is the thickness of the headgroup region, and $2D_C$ is the thickness of the tail region.

The representation of the membrane–water interface in the previous model is a simplification in that it does not account for variation of the SLD due to penetration of water into the membrane. An improvement on the three-shell model is shown in Fig. 2(C), where the innermost and outermost layers are now represented by linearly varying SLD profiles. For this model,

$$\rho(x) = \begin{cases} (\rho_{h1} - \rho_{h2})x/D_H + (\rho_{h1} - \rho_{h2})(D_H + D_C)/D_H + \rho_{h2} & \text{when } -D_C - D_H < x < -D_C, \\ \rho_c & \text{when } -D_C < x < D_C, \\ (\rho_{h2} - \rho_{h1})x/D_H + (\rho_{h1} - \rho_{h2})(D_H + D_C)/D_H + \rho_{h2} & \text{when } D_C < x < D_C + D_H, \\ \rho_m & \text{when } |x| > D_H + D_C. \end{cases}$$

Substitution of this profile into equation (9) results in

$$F_M(q) = \frac{2}{q^2 D_H} \left((\rho_{h1} - \rho_{h2}) \{ \cos(qD_C) - \cos[q(D_H + D_C)] \} + qD_H \{ (\rho_c - \rho_{h1}) \sin(qD_C) + (\rho_{h2} - \rho_m) \sin[q(D_H + D_C)] \} \right), \quad (22)$$

where ρ_{h1} is the SLD at the headgroup–water interface, ρ_{h2} is the SLD and the acyl-chain–headgroup interface, and all other variables are as before.

As an alternative to step functions, the membrane SLD profile can be represented by one or several Gaussians (Fig. 2D). For a single Gaussian, the SLD profile is given by (see *e.g.* Pabst *et al.*, 2003)

$$\rho(x) = (\rho - \rho_m) \exp(-x^2/2D_C^2), \quad (23)$$

which has a corresponding scattering amplitude given by

$$F_M(q) = (2\pi)^{1/2} (\rho - \rho_m) D_C \exp(-q^2 D_C^2/2), \quad (24)$$

where ρ is the membrane SLD, ρ_m is the solvent SLD, and D_C is the $1/e$ half-width of the membrane.

As in the case of the step-function representation, additional layers in the SLD profile can be constructed using series of Gaussians. Here, we restrict our consideration to the sum of three Gaussians (Fig. 2E), representing the outer headgroup layer, the acyl-chain region, and the inner headgroup layer. This profile is given by

$$\rho(x) = (\rho_h - \rho_m) \exp\left[-\frac{(x - X_H)^2}{2D_H^2}\right] + (\rho_c - \rho_m) \exp\left(-\frac{x^2}{2D_C^2}\right) + (\rho_h - \rho_m) \exp\left[-\frac{(x + X_H)^2}{2D_H^2}\right], \quad (25)$$

where ρ_h , ρ_c and ρ_m are the SLD of the headgroup, tail and solvent, D_H and D_C are the $1/e$ half-widths of the head and tail regions, and X_H corresponds to the center of the headgroup region with respect to the center of the bilayer. The corresponding scattering function is given by

$$F_M(q) = (2\pi)^{1/2} \left[2(\rho_h - \rho_m) D_H \exp\left(\frac{-q^2 D_H^2}{2}\right) \cos(qX_H) + (\rho_c - \rho_m) D_C \exp\left(\frac{-q^2 D_C^2}{2}\right) \right]. \quad (26)$$

Substitution of the various membrane scattering amplitudes, F_M , into equations (18) and (19) can then be used to calculate the vesicle form factor, $P(q)$, for ULVs having the membrane SLD profiles discussed above. If the monodisperse structure factor, $S(q)$, is known, then F_M [equations (18) and (19)] can also be used to determine the polydisperse structure factor, $S'(q)$. The membrane SLD profiles above can also be substituted into equation (4) to obtain analytic form factors for monodisperse vesicles. These equations are given in Appendix A.

2.5. Assessment of the SFF approximation

As mentioned above, Bartlett & Ottewill (1992) have derived an analytic expression for polydisperse core–shell spherical particles that can be easily adapted to the case of hollow shells or vesicles with a uniform membrane SLD. Comparison of scattering curves generated from the SFF and the analytic function given in Appendix B allows us to assess the relative accuracy of the SFF. Fig. 3 shows such a comparison for various values of the ratio t/R . Since the SFF

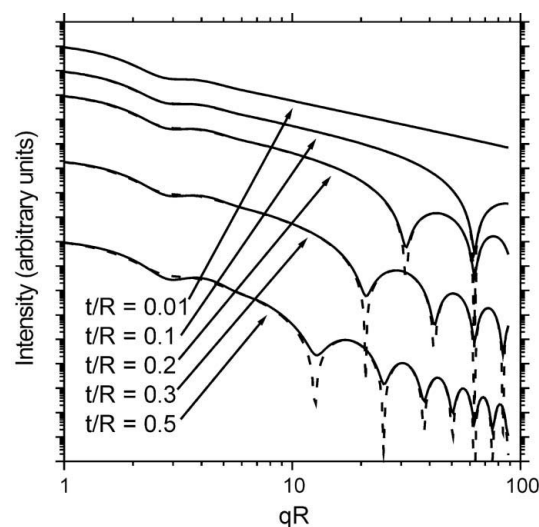


Figure 3

Comparison between analytic and SFF calculations of the polydisperse form factor for vesicles having membranes with uniform SLD. The scattering curves are plotted against the dimensionless quantity qR . For 300 Å vesicles, the q range would correspond to $0.003 < q < 0.3 \text{ \AA}^{-1}$. The relative variance or polydispersity used for each curve is the same: $1/(z + 1) = 1/16$. The analytic functions and SFF approximations are shown as solid and dashed lines, respectively. Scattering curves are plotted for several values of the ratio t/R and are shifted on the vertical scale, with t/R decreasing from bottom to top.

Table 2

Parameters used for assessment of the SFF approximation for the various SLD profiles.

SLDs have been calculated from known scattering lengths (Sears, 1992) and component volumes (Nagle & Tristram-Nagle, 2000), using the procedures described by Pencer, Mills *et al.* (2005). (n/a = not applicable.)

Model	D_{FH} (Å)	X_h (Å)	$2D_C$ (Å)	ρ_{h1} (fm Å ⁻³)	ρ_{h2} (fm Å ⁻³)	ρ_c (fm Å ⁻³)
B	10	n/a	40	2.8×10^{-7}	2.8×10^{-7}	6.9×10^{-7}
C	10	n/a	40	2.8×10^{-7}	6.4×10^{-7}	6.9×10^{-7}
D	n/a	n/a	20	n/a	n/a	6.9×10^{-7}
E	10	20	20	2.8×10^{-7}	n/a	6.9×10^{-7}

approximation depends on $t \ll R$, we expect that agreement between the SFF and the exact function will deteriorate as t/R increases. We find, in fact, that the SFF follows most of the exact function up to values $t/R \simeq 0.5$. The largest deviations between the SFF and exact scattering function occur at the minima of the scattering function corresponding to the membrane thickness. The sharpness of the minima in the case of the SFF function are due to the sharp minima in the membrane form factor. As discussed by Pencer & Hallett (2000), the curvature of the membrane surface has the effect of smearing these minima, as can be seen in the plots of the exact form factor. In practice, the deviations between the SFF and exact form factor that occur at these scattering minima will not be seen, due to additional smearing of the scattering function as a result of the instrumental resolution (see *e.g.* Glinka *et al.*, 1998).

In Fig. 4, we plot calculated scattering curves using the SFF for various model membrane SLD profiles as well as those for the exact form factors (given in Appendix A) that have been numerically integrated over the Schulz distribution. In each case, the parameters used for the calculations (summarized in

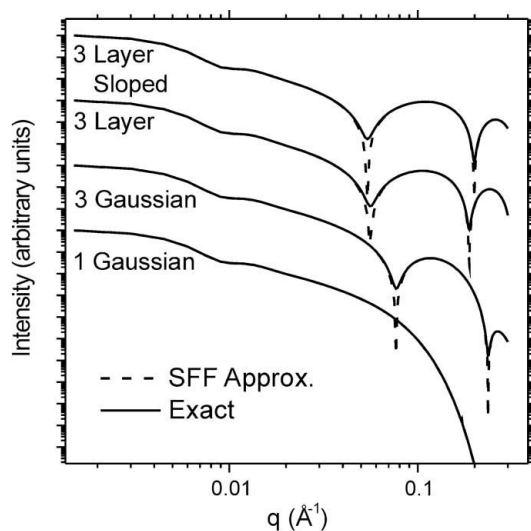


Figure 4

Comparison between analytic (solid lines) and SFF (dashed lines) calculations of the polydisperse form factor for vesicles with non-uniform membrane SLD. Calculations were performed for vesicles with a mean radius of 300 Å for the various SLD models discussed in the text. Curves are shifted on the vertical scale to facilitate viewing.

Table 2) correspond to those typical for phospholipid vesicles made up of chain perdeuterated phospholipids. We choose to use chain perdeuterated rather than hydrogenous phospholipids for the modeling, since this provides a better illustration of the contribution to the scattering function from the internal bilayer structure. Such conditions are similar to the contrast conditions one would obtain from hydrogenous phospholipid in H₂O probed by X-ray scattering. In each case, we find good agreement between the SFF and numerically integrated exact form factors, except in the vicinity of the scattering minima related to the membrane thickness.

3. Experimental procedures

3.1. Materials

1,2-Dimyristoyl-*sn*-glycero-3-phosphocholine (DMPC), 1,2-dimyristoyl-D54-*sn*-glycero-3-phosphocholine (dDMPC), and 1,2-dipalmitoyl-*sn*-glycero-3-phosphocholine (DPPC), solubilized in chloroform, were purchased from Avanti Polar Lipids, Inc. (Birmingham, AL) and used without further purification. Upon arrival, the ampules containing the various lipids were stored at 233 K. 99% purity D₂O was purchased from Cambridge Scientific (Andover, MA), while all other chemicals were reagent grade.¹

3.2. Vesicle preparation

ULVs were prepared by extrusion using the method of Nayar *et al.* (1989). Lipids solubilized in chloroform were transferred to round-bottom flasks and the chloroform was removed under a stream of N₂ followed by vacuum pumping. Lipid films were then dispersed, by agitation, into pure D₂O. The lipid dispersions were then extruded using a hand-held extruder purchased from Avanti Lipids, Inc. (Birmingham, AL). Total lipid concentrations were 10 mg ml⁻¹ prior to extrusion. ULVs were formed by successive extrusions using three polycarbonate filters of different pore diameters and a total of 27 passes [*e.g.* 200 nm (9 times), 100 nm (9 times) and 50 nm (19 times)].

3.3. Small-angle neutron scattering

SANS measurements were performed using the 30 m NG7 instrument (Glinka *et al.*, 1998) located at NIST (Gaithersburg, MD). 1.5 and 12 m sample-to-detector distances (SDD) were used along with a neutron wavelength, λ , of 8 Å ($\delta\lambda/\lambda = 10\%$), resulting in a total range in scattering vector, $q = 4\pi \sin(\theta/2)/\lambda$, of $0.004 < q < 0.3 \text{ Å}^{-1}$. SANS data were reduced and corrected for sample transmission and background using *IgorPro* (WaveMetrics, Lake Oswego, OR) with routines provided by the NIST Center for Neutron Research (NCNR). Data were fit using similar routines provided by the NCNR, which have been modified to include the models described above.

¹ Reference to commercial sources and products used in this study does not constitute endorsement by the National Institute of Standards and Technology (NIST), nor should it be inferred that the products mentioned are necessarily the best available for the purpose used.

4. Experimental results

Above, we have verified, *via* comparison with exact models and numerically integrated results, that the SFF for various SLD model profiles reproduces vesicle form factors with reasonable accuracy. Below, we demonstrate the application of the SFF approximation in fits to experimental data. Firstly, fits using the SFF and analytic forms of the scattering function for uniform shells (model A) are compared. Then the multishell SLD, model B, is used to extract membrane physical parameters for DPPC, DMPC and dDMPC, which are compared with literature values.

4.1. Validation of the SFF approximation

In Fig. 5, we show SANS data obtained from extruded DPPC ULVs in 100% D₂O at 323 K. The inset shows both the exact and the SFF fits to the data over the full q range, while the main plot shows an expanded view of the data over the high- q range. A comparison of the fit results, given in Table 3, shows close agreement between the two fits.

The close agreement between the fit results for the SFF and exact form factor is somewhat surprising, given the observation by Kiselev *et al.* (2002) of a 10% difference in vesicle radius obtained *via* fits using the two models. Considering that the difference in the fitting results given by Kiselev *et al.* (2002) corresponds to half the value of the membrane thickness, we speculate that the difference they observe between fitting results of the SFF and exact form factors could be merely an error resulting from the difference in the definition of the vesicle radius in the two models (as we have noted in Appendix B, while the radius in the SFF model corresponds to the distance between the vesicle center and bilayer midplane,

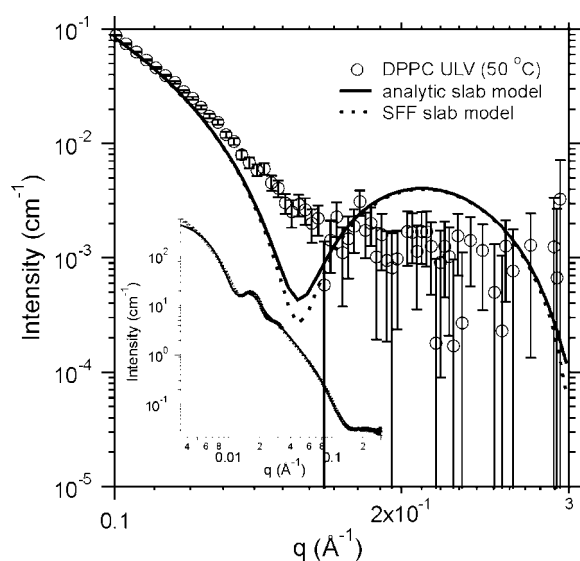


Figure 5
Fits to experimental data for DPPC ULVs at 323 K (open symbols) using the SFF approximation (dashed line) and exact form factor (solid line) for uniform shells. The inset shows the full scattering curve and both the SFF and exact fits, both including the incoherent background. The main plot shows an expanded view of the high- q data and both the SFF and exact fits, after subtraction of incoherent background.

Table 3

Fit results for DPPC ULVs measured at 273 K using the SFF approximation and exact form factors for uniform shells.

$\langle R \rangle$ and σ/R correspond to the mean radius (\AA) and the relative width of the size distribution, respectively. For all fits, the SLD, ρ_c , is assumed to be $-3.6 \times 10^{-8} \text{ fm } \text{\AA}^{-3}$.

Model	$\langle R \rangle$ (\AA)	Polydispersity ($\sigma/\langle R \rangle$)	$2D_c$ (\AA)
A (exact)	249.2 ± 0.2	0.220 ± 0.001	40.73 ± 0.03
A (SFF)	249.2 ± 0.2	0.202 ± 0.001	40.66 ± 0.03 28.5†

† Hydrophobic thickness obtained by X-ray diffraction (Nagle & Tristram-Nagle, 2000).

the vesicle radius in the exact equation given in Appendix B corresponds to distance from the vesicle center to the membrane inner surface).

Although good agreement is obtained between the SFF and exact fits for uniform ULVs, the hydrophobic thickness obtained from the fits (see Table 3) is significantly higher than that expected from complementary measurements (Nagle & Tristram-Nagle, 2000). While, on the one hand, the high contrast between the lipid acyl chains and D₂O should make the hydrophobic thickness the main contribution to the scattering function, the lipid–water interface may also make a non-negligible contribution. As can be seen in Fig. 5, both functions deviate from the experimental data at high q ($q > \sim 0.12 \text{ \AA}^{-1}$). In fact, the contribution of the lipid–water interface produces both the discrepancy between the models and experimental data and the overestimate in the hydrophobic thickness (see *e.g.* Kučerka *et al.*, 2004). As will be shown below, approximation of the SLD by a multishell model, rather than single-shell model, improves the agreement between the model scattering curves and experimental data at high q and results in better estimates of hydrophobic thicknesses.

4.2. Determination of membrane structural parameters

The merits of various SLD model profiles have been discussed in detail by *e.g.* Wiener & White (1992), Nagle & Tristram-Nagle (2000), Kučerka *et al.* (2004) and Kiselev, Zemlyanaya & Aswal, (2004). Furthermore, Kučerka *et al.* (2004) have shown that the quality of fits using the SLD model B and variations of model C are essentially equivalent. Here, we use model B to represent the membrane SLD, since it requires the least number of parameters while still incorporating distinct regions to represent the lipid headgroups and acyl chains.

Fig. 6 shows SANS data obtained from ULVs composed of DPPC, DMPC and dDMPC in 100% D₂O. Measurements of SANS from DPPC ULVs were obtained at 323 K, while those from DMPC and dDMPC were obtained at 303 K. Initially, fits to the data were attempted where the headgroup and acyl-chain thicknesses and SLDs were unconstrained. We found that it was not possible to obtain unique solutions to fits with this number of parameters unconstrained. In order to obtain reproducible fits to the experimental data, we followed the procedure and constraints described by Kučerka *et al.* (2004).

Table 4

Constrained parameters used in fits to SANS data from DPPC (at 323 K), DMPC and dDMPC ULVs (both at 303 K).

The lipid headgroup volume is assumed to be the same for all three lipids.

Component	Chemical formula	V (\AA^3)	B (fm)
Water	H ₂ O	30	-1.68
Heavy water	D ₂ O	29.9	19.15
PC headgroup	C ₁₀ H ₁₈ NO ₈ P	319	60.1
DPPC chains	C ₃₀ H ₆₂	913	-32.4
DMPC chains	C ₂₆ H ₅₄	782	-29.1
dDMPC chains	C ₂₆ D ₅₄	782	533

As in the work of Kučerka *et al.* (2004), we parse the lipid membrane into three layers: an inner headgroup layer, consisting of the carbonyl groups, glycerol backbone, phosphate and choline; a lipid acyl-chain region, consisting of the terminal methyl and methylene groups of the hydrocarbon chains; and an outer headgroup, which is chemically identical to the inner headgroup. For the hydrocarbon region, we constrain the SLD, $\rho_C = B_C/V_C$, based on literature values for the scattering lengths, B (Sears, 1992), and acyl-chain molecular volumes, V (Nagle & Tristram-Nagle, 2000). The SLD of the lipid headgroup region, ρ_H , is calculated assuming that the headgroup region contains both the lipid headgroups themselves and water that has penetrated into the membrane. If n'_W waters are associated with a single headgroup, then the SLD of the headgroup region is $\rho_H = (B_H + n'_W B_W)/(V_h + n'_W V_W)$. Finally, the lengths of the acyl-chain and headgroup regions can be related *via* the lipid cross-sectional area, A_L , to give (Kučerka *et al.*, 2004)

$$A_L = \frac{V_H + n'_W V_W}{D_P} = \frac{V_C}{D_C}. \quad (27)$$

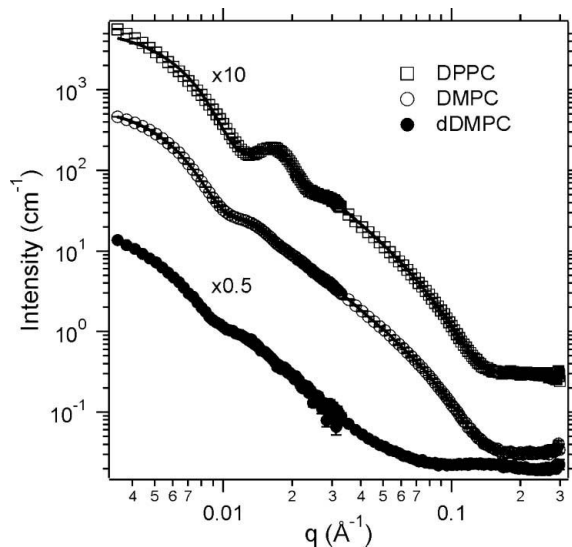


Figure 6

Fits to experimental data using SLD model B with the SFF approximation. Open squares correspond to DPPC SANS data (taken at 323 K), open circles to DMPC and solid circles to dDMPC (both taken at 303 K). Solid lines correspond to fits to the data. The fitting results are summarized in Table 5.

Table 5

Results of fits to SANS data from DPPC ULVs (at 323 K), DMPC and dDMPC ULVs (both at 303 K), using multishell model B.

Sample	n'_W	A_L (\AA^2)	D_H (\AA)	$2D_C$ (\AA)	D_L (\AA)
DPPC	16.5 ± 0.4	58.0 ± 2.2	14.0 ± 0.2	31.5 ± 1.2	59.5 ± 1.6
DPPC†	8.6	64	9	28.5	46.5
DMPC	24.3 ± 0.3	56.5 ± 1.0	18.5 ± 0.1	27.6 ± 0.5	64.6 ± 0.7
dDMPC	20.1 ± 6.8	50 ± 21	18.5 ± 1.7	32 ± 14	69 ± 17
DMPC†	7.2	59.6	9	26.2	44.2

† Literature values for lipid structural parameters (Nagle & Tristram-Nagle, 2000).

Use of the constraints above reduces the number of fitting parameters of the multishell model from 4, namely the headgroup and acyl-chain thicknesses and SLDs, to 2, namely the number of waters located within the headgroup region, n'_W , and thickness of the headgroup region, D_H . The component volumes and scattering lengths used below are summarized in Table 4. The total lipid volumes are 1232 and 1101 \AA^3 for DPPC at 323 K and DMPC at 303 K, respectively.

The full SANS curves for DPPC ULV (taken at 323 K), DMPC and dDMPC ULV (both taken at 303 K) are shown in Fig. 6 and expanded plots of the high- q data after background subtraction are shown in Fig. 7. Also shown in both figures are fits to the data using model B, as described above. The various structural parameters extracted from the fits are summarized in Table 5, along with values obtained by complementary techniques (see *e.g.* Nagle & Tristram-Nagle, 2000).

Comparison of the fits in Fig. 7 with those of Fig. 5 shows that the multishell model, B, gives a better fit to the data at high q than the single-shell model, A. However, the fits still deviate from the experimental data beyond $q > \sim 0.17 \text{\AA}^{-1}$, suggesting that some improvements could still be made in the

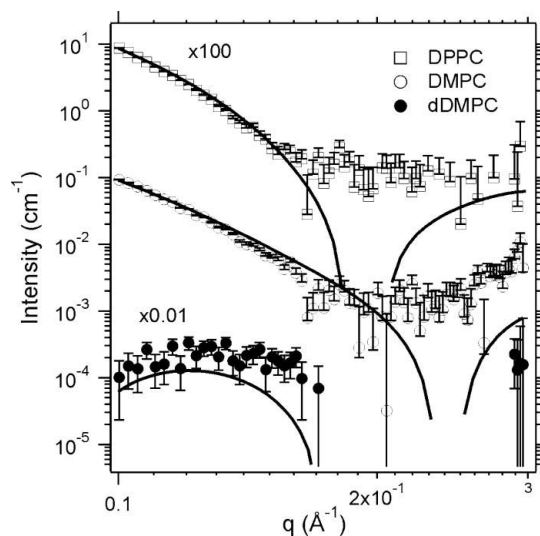


Figure 7

Expanded view of fits shown in Fig. 6. Fits to experimental data using SLD model Cii with the SFF approximation. Open squares correspond to DPPC SANS data (taken at 323 K), open circles to DMPC and solid circles to dDMPC (both taken at 303 K). Solid lines correspond to fits to the data. Data are shown after subtraction of incoherent background. Fitting parameters are given in Table 5. Note that the gap in the data from dDMPC is a result of an overestimate of the fit to the incoherent background in this q range.

model SLD profile. In comparing fit results with literature values, we find that, while we obtain reasonable values for the lipid hydrophobic thickness for all three lipids, the fits significantly overestimate the lipid headgroup thickness and number of hydrating waters. These overestimates lead to both an exaggerated total lipid thickness and an underestimated area per lipid. Consequently, while the multishell model is useful for determination of the membrane hydrophobic thickness from small-angle scattering measurements, additional improvements should be made to the SLD model used in order to obtain more reasonable values for the other membrane parameters, such as the lipid headgroup thickness and degree of hydration. Detailed examination of possible improvements to model SLD profiles is beyond the scope of this work; nevertheless, the use of the polydisperse SFF should facilitate this exercise.

5. Conclusions

We have extended the previously derived SFF approximation to include an analytic form for Schultz- or Gamma-distributed ULVs using a straightforward Laplace transform. In assessing this extended SFF approximation, we have found the SFF to be robust, closely following the exact expression for polydisperse ULVs with uniform shells up to values of $t/R = 0.5$. For various SLD profiles using typical parameters for phospholipid ULVs, the SFF closely follows the exact form factors (numerically integrated over the Schulz distribution).

As expected from comparisons with numerical calculations, for ULVs with uniform membrane SLD, we find that the polydisperse SFF is reasonably robust in fitting the experimental data, giving essentially the same results as fits to the analytic function. We have also confirmed results from previous studies (e.g. Kučerka *et al.*, 2004; Kiselev, Zbytovská *et al.*, 2004) that the representation of the ULV membrane SLD as a homogeneous layer (*i.e.* single-shell model) does not adequately describe the experimental scattering data. Through the use of a multishell model, we are able to improve the fits to experimental data and obtain reasonable values for membrane hydrophobic thicknesses. However, further improvements to the model SLD profile are necessary in order to improve on the values of the other membrane parameters (e.g. headgroup thickness, number of hydrating waters, *etc.*). The utility of the polydisperse SFF should stimulate further investigations of ULV structural parameters (e.g. Kiselev, Zbytovská *et al.*, 2004; Kiselev, Zemlyanaya & Aswal, 2004; Kučerka *et al.*, 2004; Pencer, Nieh *et al.*, 2005).

APPENDIX A

Exact form factors for monodisperse vesicles

Above, we have used the various model membrane SLD profiles to derive membrane form factors, for use in the SFF approximation. It is also possible, however, to derive exact expressions for the form factors for monodisperse vesicles by

substituting the various SLD profiles into equation (4). These expressions are provided below.

A1. The uniform shell

$$P(q) = (\rho - \rho_m)^2 \left[R_0^3 \frac{j_1(qR_0)}{qR_0} - R_i^3 \frac{j_1(qR_i)}{qR_i} \right]^2, \quad (28)$$

where ρ is the membrane SLD, ρ_m is the SLD of the medium, R is the average vesicle radius, t is the thickness, $R_0 = R + t/2$, $R_i = R - t/2$, and $j_1(x)$ is the first-order spherical Bessel function, expressed as

$$j_1(x) = \frac{\sin(x)}{x^2} - \frac{\cos(x)}{x}. \quad (29)$$

A2. The three-layer shell – uniform layers

$$P(q) = \left\{ \sum_{i=1}^3 \rho_i \left[R_i^3 \frac{j_1(qR_i)}{qR_i} - R_{i-1}^3 \frac{j_1(qR_{i-1})}{qR_{i-1}} \right] \right\}^2, \quad (30)$$

where R is the average ULV radius. $2D_C$ and D_H are the thicknesses of the acyl-chain and headgroup layers, respectively,

$$\begin{aligned} R_3 &= R + D_H + D_C, & \rho_3 &= \rho_h - \rho_m, \\ R_2 &= R + D_C, & \rho_2 &= \rho_c - \rho_m, \\ R_1 &= R - D_C, & \rho_1 &= \rho_3, \\ R_0 &= R - D_H - D_C, \end{aligned}$$

ρ_h is the headgroup region SLD, ρ_c is the acyl-chain region SLD, and ρ_m is the SLD of the medium.

A3. The three-layer shell – linearly varying SLDs

$$P(q) = \left\{ \sum_{i=1}^3 \rho_i \left[R_i^3 \frac{j_1(qR_i)}{qR_i} - R_{i-1}^3 \frac{j_1(qR_{i-1})}{qR_{i-1}} \right] + \rho_a [F_1(qR_1) - F_1(qR_0)] + \rho_b [F_1(qR_3) - F_1(qR_2)] \right\}^2, \quad (31)$$

where

$$F_1(qR) = \frac{2R \sin(qR)}{q^3} - \frac{(q^2 R^2 - 2) \cos(qR)}{q^4}. \quad (32)$$

R is the average ULV radius. D_C and D_H are the thicknesses of the acyl-chain and headgroup layers, respectively,

$$\begin{aligned}
 R_3 &= R + D_H + 2D_C, \\
 R_2 &= R + D_C, \\
 R_1 &= R - D_C, \\
 R_0 &= R - D_H - D_C, \\
 \rho_3 &= \rho_{h2} - \rho_m - (\rho_{h1} - \rho_{h2})(R - D_H - D_C)/D_H, \\
 \rho_2 &= \rho_c - \rho_m, \\
 \rho_1 &= \rho_{h2} - \rho_m - (\rho_{h2} - \rho_{h1})(R + D_H + D_C)/D_H, \\
 \rho_a &= (\rho_{h1} - \rho_{h2})/D_H, \\
 \rho_b &= (\rho_{h2} - \rho_{h1})/D_H,
 \end{aligned}$$

ρ_{h2} is the headgroup–water interface SLD, ρ_{h1} is the headgroup–acyl-chain region interface SLD, ρ_c is the acyl-chain region SLD and ρ_m is the SLD of the medium.

A4. The single Gaussian profile

$$\begin{aligned}
 P(q) &= \frac{2\pi D_C^2}{q^2} (\rho - \rho_m)^2 \exp(-D_C^2 q^2) [D_C^2 q \cos(qR) \\
 &\quad + R \sin(qR)]^2, \tag{33}
 \end{aligned}$$

where ρ is the membrane SLD, ρ_m is the SLD of the medium, and D_C is the $1/e$ half-width of the membrane.

A5. The sum of Gaussians

$$\begin{aligned}
 P(q) &= \frac{2\pi}{q^2} \left(\sum_{i=1}^3 (\rho_i - \rho_m) d_i \exp(-d_i^2 q^2 / 2) \right. \\
 &\quad \left. \times \{d_i^2 q \cos[q(R + X_i)] + (R + X_i) \sin[q(R + X_i)]\} \right)^2, \tag{34}
 \end{aligned}$$

where

$$\begin{aligned}
 d_3 &= D_H, & \rho_3 &= \rho_h - \rho_m, \\
 d_2 &= 2D_C, & \rho_2 &= \rho_c - \rho_m, \\
 d_1 &= D_3, & \rho_1 &= \rho_3, \\
 X_3 &= X_H, \\
 X_2 &= 0, \\
 X_1 &= -X_3,
 \end{aligned}$$

ρ_h, ρ_c and ρ_m are the SLDs of the headgroup, tail and medium, D_H and $2D_C$ are the $1/e$ half-widths of the head and tail regions, and X_H corresponds to the center of the headgroup region with respect to the center of the bilayer.

APPENDIX B

Exact form factor for polydisperse core–shell spherical particles

Below, we provide the analytic form factor for polydisperse core–shell particles, as found in the work by Bartlett & Ottewill (1992).

$$\begin{aligned}
 P(\bar{x}) &= \frac{16\pi^2}{q^6} (\rho_s - \rho_c)^2 \left(c_1 + c_2 \bar{x} + c_3 \bar{x}^2 \left(\frac{z+2}{z+1} \right) \right. \\
 &\quad + B(\bar{x})^{(z+1)/2} \{c_4 \cos[(z+1)D(\bar{x})] + c_7 \sin[(z+1)D(\bar{x})]\} \\
 &\quad + \bar{x} B(\bar{x})^{(z+2)/2} \{c_5 \cos[(z+2)D(\bar{x})] + c_8 \sin[(z+2)D(\bar{x})]\} \\
 &\quad + \left(\frac{z+2}{z+1} \right) \bar{x}^2 B(\bar{x})^{(z+3)/2} \\
 &\quad \left. \times \{c_6 \cos[(z+3)D(\bar{x})] + c_9 \sin[(z+3)D(\bar{x})]\} \right), \tag{35}
 \end{aligned}$$

where $\bar{x} = qr_c$, r_c is the average radius of the core (which is related to the average radius r_a given earlier in the text by $r_c + D_C = r_a$), the functions $B(\bar{x})$ and $D(\bar{x})$ are defined as

$$B(\bar{x}) = \frac{(z+1)^2}{(z+1)^2 + 4\bar{x}^2}, \tag{36}$$

and

$$D(\bar{x}) = \tan^{-1} \left(\frac{2\bar{x}}{z+1} \right), \tag{37}$$

and the coefficients c_i are given by

$$\begin{aligned}
 c_1 &= \frac{1}{2} - \gamma(\cos y + y \sin y) + \frac{\gamma}{2}(1 + y^2), \\
 c_2 &= \gamma y(\gamma - \cos y), \\
 c_3 &= \frac{\gamma^2 + 1}{2} - \gamma \cos y, \\
 c_4 &= \gamma^2 (y \cos y - \sin y)^2 - c_1, \\
 c_5 &= 2\gamma \sin y [1 - \gamma(y \sin y + \cos y)], \\
 c_6 &= c_3 - \gamma^2 \sin^2 y, \\
 c_7 &= \gamma \sin y - \frac{\gamma^2}{2}(1 + y^2) \sin 2y - c_5, \\
 c_8 &= c_4 - \frac{1}{2} + \gamma \cos y - \frac{\gamma^2}{2}(1 + y^2) \cos 2y, \\
 c_9 &= \gamma \sin y (1 - \gamma \cos y), \tag{38}
 \end{aligned}$$

where $y = 2qD_C$, $2D_C$ is the shell thickness, $\gamma = (\rho_m - \rho_s)/(\rho_c - \rho_s)$, ρ_m is the SLD of the medium, ρ_s is the SLD of the shell, and ρ_c is the SLD of the core. For the situation considered here (hollow shells), $\rho_c = \rho_m$ and $\gamma = 1$.

The authors thank T. A. Harroun and M.-P. Nieh for useful discussions. We acknowledge the support of the National Institute of Standards and Technology, US Department of Commerce, in providing the neutron research facilities used in this work. JP, JK and CPA thank The Advanced Foods and Materials Network (Networks of Centres of Excellence, Canada) for financial assistance. This study was also performed in part with support from the National Institutes of Health grant No. 1 R01 RR14812 and the Regents of the University of California through contributions from the Cold Neutrons for Biology and Technology (CNBT) research

partnership. We also thank Avanti Polar Lipids, Inc., for providing the space-filling model of the phospholipid used in Fig. 1.

References

- Alberts, B., Bray, D., Lewis, J., Raff, M., Roberts, K. & Watson, J. D. (1989). *Molecular Biology of the Cell*. New York: Garland Publishing.
- Aragón, S. R. & Pecora, R. (1976). *J. Chem. Phys.* **64**, 2395–2404.
- Bartlett, P. & Ottewill, R. H. (1992). *J. Chem. Phys.* **96**, 3306–3318.
- Ben-Shooshan, I., Kessel, A., Ben-Tal, N., Cohen-Luria, R. & Parola, A. H. (2002). *Biochim. Biophys. Acta*, **1587**, 21–30.
- Brzustowicz, M. R. & Brunger, A. T. (2005). *J. Appl. Cryst.* **38**, 126–131.
- Darkes, M. J. M. & Bradshaw, J. P. (2000). *Acta Cryst.* **D56**, 48–54.
- Dumas, F., Lebrun, M. C. & Tocanne, J.-F. (1999). *FEBS Lett.* **458**, 271–277.
- Glinka, C. J., Barker, J. G., Hammouda, B., Krueger, S., Moyer, J. J. & Orts, W. J. (1998). *J. Appl. Cryst.* **31**, 430–441.
- Gregoriadis, G. (1995). *TIBTECH*, **13**, 527–537.
- Hallett, F. R., Nickel, B., Samuels, C. & Krygsman, P. H. (1991). *J. Electron Microsc. Tech.* **17**, 459–466.
- Hallett, F. R., Watton, J. & Krygsman, P. H. (1991). *Biophys. J.* **59**, 357–362.
- Hayter, J. B. (1983). *Physics of Amphiphiles: Micelles, Vesicles and Microemulsions*, edited by V. Degiorgio & M. Corti, pp. 59–93. Amsterdam: North-Holland.
- Hristova, K. & White, S. H. (1998). *Biophys. J.* **74**, 2419–2433.
- Jacobs, R. E. & White, S. H. (1989). *Biochemistry*, **28**, 3421–3437.
- Katsaras, J., Yang, D. S.-C. & Epand, R. M. (1992). *Biophys. J.* **63**, 1170–1175.
- Killian, J. A. (1998). *Biochim. Biophys. Acta*, **1376**, 401–416.
- King, G. I., Jacobs, R. E. & White, S. H. (1985). *Biochemistry*, **24**, 4637–4645.
- Kiselev, M. A., Lesieur, P., Kisselev, A. M., Lombardo, D. & Aksenov, V. L. (2002). *Appl. Phys. A*, **74**(Suppl.), S1654–S1656.
- Kiselev, M. A., Zbytovská, J., Matveev, D., Wartewig, S., Gapienko, I. V., Perez, J., Lesieur, P., Hoell, A. & Neubert, R. (2004). *Collect. Surf. A*, **256**, 1–7.
- Kiselev, M. A., Zemlyanaya, E. V. & Aswal, V. K. (2004). *Crystal. Rep.* **49**(Suppl. 1), S136–S141.
- Korgel, B. A. & Monbouquette, H. G. (2000). *Langmuir*, **16**, 3588–3594.
- Kotlarchyk, M. & Chen, S.-H. (1983). *J. Chem. Phys.* **79**, 2461–2469.
- Kučerka, N., Nagle, J. F., Feller, S. E. & Balgavý, P. (2004). *Phys. Rev. E*, **69**, 051903(1–7).
- Marsan, M. P., Bellet-Amalric, E., Muller, I., Zaccari, G. & Milon, A. (1998). *Biophys. Chem.* **75**, 45–55.
- Marsh, D. (2002). *Eur. Biophys. J.* **31**, 559–562.
- Nagle, J. F. & Tristram-Nagle, S. (2000). *Biochim. Biophys. Acta*, **1469**, 159–195.
- Nayar, R., Hope, M. J. & Cullis, P. R. (1989). *Biochim. Biophys. Acta*, **986**, 200–206.
- Nieh, M.-P., Raghunathan, V. A., Kline, S. R., Harroun, T. A., Huang, C.-Y., Pencer, J. & Katsaras, J. (2005). *Langmuir*, **21**, 6656–6661.
- Pabst, G., Koschuch, R., Pozo-Navas, B., Rappolt, M., Lohner, K. & Laggner, P. (2003). *J. Appl. Cryst.* **36**, 1378–1388.
- Pencer, J. & Hallett, F. R. (2000). *Phys. Rev. E*, **61**, 3003–3008.
- Pencer, J. & Hallett, F. R. (2003). *Langmuir*, **19**, 7488–7497.
- Pencer, J., Mills, T., Anghel, V., Krueger, S., Epand, R. M. & Katsaras, J. (2005). *Euro. Phys. J. E*, **18**, 447–458.
- Pencer, J., Nieh, M.-P., Harroun, T., Krueger, S., Adams, C. & Katsaras, J. (2005). *Biochim. Biophys. Acta*, **1720**, 84–91.
- Raghunathan, V. A. & Katsaras, J. (1995). *Phys. Rev. Lett.* **74**, 4456–4459.
- Ridder, A. N. J. A., van de Hoef, W., Stam, J., Kuhn, A., de Kruijff, B. & Killian, J. A. (2002). *Biochemistry*, **41**, 4946–4952.
- Riske, K. A., Amaral, L. Q. & Lamy-Freund, M. T. (2001). *Biochim. Biophys. Acta*, **1511**, 297–308.
- Schmiedel, H., Jörchel, P., Kiselev, M. & Klose, G. (2001). *J. Phys. Chem. B*, **105**, 111–117.
- Sears, V. F. (1992). *Neutron News*, **3**, 26.
- Wagner, J. (2004). *J. Appl. Cryst.* **37**, 750–756.
- Wiener, M. C. & White, S. H. (1992). *Biophys. J.* **61**, 434–447.
- Wilkins, M. H. F., Blaurock, A. E. & Engelman, D. M. (1971). *Nature New Biol.* **230**, 72–76.
- Worcester, D. L. & Franks, N. P. (1976). *J. Mol. Biol.* **100**, 359–378.
- Zbytovská, J., Kiselev, M. A., Funari, S. S., Garamus, V. M., Wartewig, S. & Neubert, R. (2005). *Chem. Phys. Lipids*, **138**, 69–80.